AD-A185 549 CHARACTERIZATION OF MECHANICAL DAMAGE MECHANISMS IN CERAMIC COMPOSITE MATERIALS(U) SOUTHWEST RESEARCH INST SAN ANTONIO TX J LANKFORD AUG 87 SWRI-06-8124 1/1

UNCLASSIFIED N00014-84-C-0213 F/G 11/2 NL

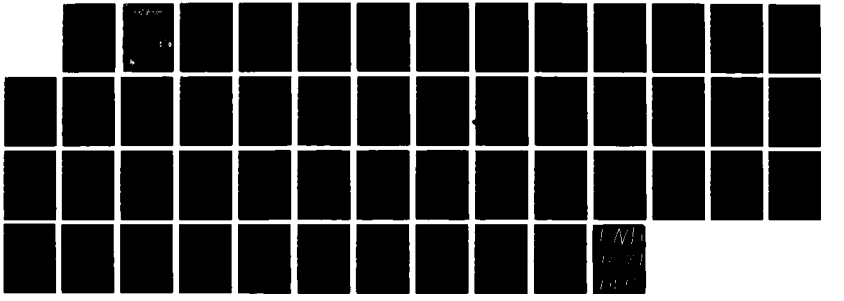

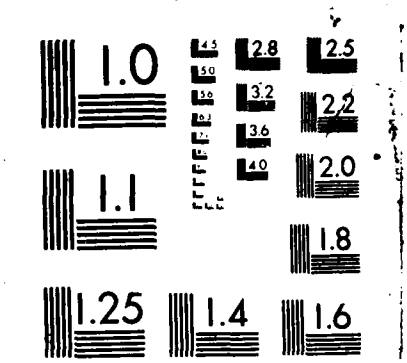

(12)

CHARACTERIZATION OF MECHANICAL DAMAGE MECHANISMS IN CERAMIC COMPOSITE MATERIALS

By
James Lankford, Jr.

TECHNICAL REPORT
ONR CONTRACT NO. N00014-84-C-0213
ONR Contract Authority NR 032-553
SwRI-8124

For
Office of Naval Research
Arlington, VA 22217

By
Southwest Research Institute
San Antonio, Texas

August 1987

SOUTHWEST RESEARCH INSTITUTE
SAN ANTONIO HOUSTON

UNCLASSIFIED
SECURITY CLASSIFICATION OF THIS PAGE

REPORT DOCUMENTATION PAGE

AD-A185 549

1a. REPORT SECURITY CLASSIFICATION Unclassified	1b. RESTRICTIVE MARKINGS
2a. SECURITY CLASSIFICATION AUTHORITY	3. DISTRIBUTION/AVAILABILITY OF REPORT Distribution Unlimited
2b. DECLASSIFICATION/DOWNGRADING SCHEDULE	
4. PERFORMING ORGANIZATION REPORT NUMBER(S) 06-8124	5. MONITORING ORGANIZATION REPORT NUMBER(S) NR 032-553
6a. NAME OF PERFORMING ORGANIZATION Southwest Research Institute 6b. OFFICE SYMBOL (If applicable)	7a. NAME OF MONITORING ORGANIZATION Dr. Steven G. Fishman - Code 431N Office of Naval Research
6c. ADDRESS (City, State, and ZIP Code) 6220 Culebra Road, P.O. Drawer 28510 San Antonio, TX 78284.	7b. ADDRESS (City, State, and ZIP Code) 800 North Quincy Street Arlington, VA 22217
8a. NAME OF FUNDING/SPONSORING ORGANIZATION Office of Naval Research 8b. OFFICE SYMBOL (If applicable)	9. PROCUREMENT INSTRUMENT IDENTIFICATION NUMBER N00014-84-C-0213
8c. ADDRESS (City, State, and ZIP Code) 800 North Quincy Street Arlington, VA 22217	10. SOURCE OF FUNDING NUMBERS PROGRAM ELEMENT NO. / PROJECT NO. / TASK NO. / WORK UNIT ACCESSION NO.

11. TITLE (Include Security Classification)
Characterization of Mechanical Damage Mechanisms in Ceramic Composite Materials

12. PERSONAL AUTHOR(S)
James Lankford

13a. TYPE OF REPORT	13b. TIME COVERED	14. DATE OF REPORT (Year, Month, Day)	15. PAGE COUNT
Technical	FROM 05/24/86 TO 05/23/87	August 1987	

16 SUPPLEMENTARY NOTATION

17 COSATI CODES		
FIELD	GROUP	SUB-GROUP

18. SUBJECT TERMS (Continue on reverse if necessary and identify by block number)
Key Words: compressive strength; partially stabilized zirconia; temperature effects; composite materials; fracture mechanisms; ceramics; plastic flow; glass matrix ceramics; cavitation.

19 ABSTRACT (Continue on reverse if necessary and identify by block number)

Earlier work on compressive strength of glass-ceramic matrix SiC fiber-reinforced composites is extended to define their behavior at high strain rates, and to assess the role of matrix phase versus fibers under such conditions. It is shown that the composite material can possess extremely high strain rate hardening exponents for strain rates in excess of about 400/s. These uniquely rapid increases in strength are found to depend upon composite microstructure and its orientation relative to the load axis; specifically, such strengthening correlates with at least one major set of fiber bundles being parallel to the load axis. The latter fail by kink initiation and propagation, a highly strain rate-dependent, temperature-independent process. For off-axis impulsive-load situations, the pyroceram matrix itself plays a significant role in controlling failure.

(Continued)

20. DISTRIBUTION/AVAILABILITY OF ABSTRACT ☒ UNCLASSIFIED/UNLIMITED ☐ SAME AS RPT ☐ DTIC USERS	21. ABSTRACT SECURITY CLASSIFICATION Unclassified
22a NAME OF RESPONSIBLE INDIVIDUAL James Lankford	22b TELEPHONE (Include Area Code) 512/522-2317 22c. OFFICE SYMBOL

DD FORM 1473, 84 MAR 83 APR edition may be used until exhausted.
All other editions are obsolete.

SECURITY CLASSIFICATION OF THIS PAGE
UNCLASSIFIED

19. Recent experimental work on the yield and flow behavior of both single crystal and polycrystalline transformation toughened zirconia is presented. In addition, related work by other researchers is reviewed. The resulting picture is used to assess the relative plastic deformation contributions of phase transformations, dislocation activity, and grain boundary sliding. Particular emphasis is placed on the effects of stabilizer chemistry, grain size, temperature, strain rate, and state of stress. The results are shown to reflect the strong role of shear stresses in selecting, and controlling the operation of, each deformation mode.

FOREWORD

This report describes recent work carried out under an experimental program aimed at characterizing damage mechanisms and compressive failure in ceramic-matrix composite materials. The report consists of two papers, each having been submitted to the journal noted on its title page.

TABLE OF CONTENTS

LIST OF ILLUSTRATIONS

Ceramic Engineering And Science Proceedings (submitted)

I.

STRENGTH OF MONOLITHIC AND FIBER-REINFORCED GLASS CERAMICS AT HIGH RATES OF LOADING AND ELEVATED TEMPERATURE

James Lankford

Southwest Research Institute
San Antonio, TX 78284

Abstract

Earlier work on compressive strength of glass-ceramic matrix SiC fiber-reinforced composites is extended to define their behavior at high strain rates, and to assess the role of matrix phase versus fibers under such conditions. It is shown that the composite material can possess extremely high strain rate hardening exponents for strain rates in excess of about 400 s^{-1}. These uniquely rapid increases in strength are found to depend upon composite microstructure and its orientation relative to the load axis; specifically, such strengthening correlates with at least one major set of fiber bundles being parallel to the load axis. The latter fail by kink initiation and propagation, a highly strain rate-dependent, temperature-independent process. For off-axis impulsive-load situations, the pyroceram matrix itself plays a significant role in controlling failure.

I. INTRODUCTION

Recently it was shown[1] that ceramic fiber-reinforced ceramic matrix composites can exhibit remarkable strengthening effects when subjected to rapid compressive loading. The amplitude of, and strain rate threshold for, this behavior depends sensitively upon fiber layup, orientation relative to the load axis, and temperature. Failure under such conditions was shown to be a complex process, involving matrix microfracture or flow, fiber kinking or buckling, and shear fault propagation. During the course of interpreting these earlier observations, however, several questions arose, and are the subject of the present paper.

A major point of concern is the magnitude of the strain rate hardening exponent (n) within the dynamic strain rate regime ($10^2 < \dot{\varepsilon} < 10^4 s^{-1}$) characteristic of the Hopkinson pressure bar (HPB) test apparatus. Existing dynamic failure theory[2] is based on the assumption of a monolithic brittle specimen, within which microfracture is controlled by crack inertia. Modeling this situation yields predicted n-values on the order of 0.33, which have indeed been measured for some monolithic ceramics and rocks. However, limited testing[1] of SiC fiber reinforced lithium-aluminosilicate (LAS) ceramic-glass matrix composites suggested that for certain variants of this system, n could be as high as 0.45. This is extremely important, since it means that as the rate of loading increases, the strength of the composite rises very rapidly. However, this earlier data was obtained for only a limited HPB range, so that evaluation of the strain rate exponent was only approximate. In the present work, the results of experiments are reported in which specimens of various microstructures and orientation are tested at several

temperatures over a sufficiently broad range in pressure bar loading rate to accurately characterize the dynamic value(s) of n.

A closely related issue concerns the dynamic behavior of the matrix material itself, since it appears that composite degradation is preceded by matrix microfracture or yielding. To date, strain rate exponents for most monolithic ceramics (Al_2O_3, SiC, HP Si_3N_4) tested in the HPB[3,4] have ranged from a maximum of -0.33 to near zero, depending upon whether or not the threshold for inertial strengthening is exceeded. Furthermore, if transgranular microfracture is suppressed at elevated temperatures by intergranular sliding, crack inertia may be rendered inoperative. This is most likely to occur in fine-grained ceramics with glassy grain boundaries. Whatever the magnitude of n for the matrix phase, any difference between this value and that measured for the composite must be attributed to additional or alternative damage mechanisms characteristic of the specific composite microstructure.

Finally, it is relevant to compare compressive behavior with tensile and flexural failure since the latter reflects a combination of tensile and compressive damage. To this end, the present compression results will be compared with earlier tension and flexure experiments by Prewo[5].

II. EXPERIMENTAL

II.1 Material Characterization

The basic composite materials investigated in this study were obtained in the form of Compglas panels consisting of a pyroceramic matrix, reinforced with ~ 46 v/o, 15 μm diameter SiC fibers oriented unidirectionally (0° orientation), or cross-plied from 200 μm thick laminates of parallel fibers, with the bundles laid up normal to another. The matrix material was composed of lithium-aluminosilicate (LAS) glass-ceramic, samples of which were obtained in the form of as-ceramed monolithic bodies. These monolithic and matrix phases differed slightly, as described below.

The specific pyrocerams used in this study have been characterized microstructurally by Larsen[6] and by Brennan[7]. In the case of the monolithic material, 3 w/o TiO_2 is included as a nucleating agent, with the predominant phase being crystalline $(Li_2O{\cdot}MgO) \cdot Al_2O_3 \cdot n\ SiO_2$ ($n > 3.5$); the grain size for this phase was uniform, and on the order of 1 μm. Also present were occasional blocky crystals of mullite ($3Al_2O_3 \cdot 2SiO_2$). A residual glassy phase, on the order of 5%, remained at the grain boundaries. The composite matrix material was very similar, but with 3 w/o ZrO_2 replacing the TiO_2, and ~ 5 w/o Nb_2O_5 added for NbC reaction barrier formation at the matrix-SiC fiber interface. Phase structures were nearly identical to those of he monolithic material, aside from the added presence of occasional needle-shaped $ZrSiO_4$ crystals and slightly larger (0.5 - 2 μm) predominant grains. The smallest grains were located near the fiber-matrix interface.

II.2. Test Procedures

The experimental approach used has been described in detail elsewhere[8], and is briefly outlined here. Cylindrical specimens (12 mm long x 6 mm diameter) for compression testing were machined from the as-received composite panels, or from the monolithic ceramic matrix bodies. For the 0° specimens, the cylinder axis was parallel to the fibers, while for the crossplied material, two stress axis orientations were chosen. In the first case, the cylinder was aligned parallel to one set of fibers, and normal to the other (0/90); in the second, the compression axis was oriented at 45° to both sets of fibers (45/45). Monolithic pyroceram specimens were machined from a single ceramic body, all with the same axial orientation relative to the body.

All specimens were tested in air at temperatures ranging from 23°C to 1100°C. Tests at strain rates of ~ $10^{-4}s^{-1}$ and $10^{0}s^{-1}$ were performed in a standard servo-controlled hydraulic test machine, while rates on the order of $10^{3}s^{-1}$ were obtained by means of a split Hopkinson pressure bar apparatus. Small nickel-base superalloy rings were honed so as to just fit over the ends of each composite specimen, to prevent brooming[8].

In order to vary the HPB stress rate, the velocity of the pressure bar striker was varied over a wide range. Strain rate was calculated by dividing the stress rate by the temperature-corrected elastic modulus of the specimen.

Specimen stress-strain curves were obtained at low and intermediate rates by recording crosshead displacement. In addition, acoustic emission (AE) was characterized at low $\dot{\varepsilon}$ by using a transducer

resonant at 160 kHz; the latter was attached to the alumina loading platens outside the hot zone of the test furnace. Damage introduced by compressive loading was characterized by optical and scanning election microscopy of sections of damaged but unfailed specimens. This extensive work is being reported in a separate paper[9], and will be referenced in the present work.

III. RESULTS

The Compglas material exhibited two distinct modes of behavior at high strain rates; these were essentially independent of temperature, but strongly dependent upon fiber layup and orientation. Plotted in Fig. 1a is compressive failure strength σ_c versus $\dot{\varepsilon}$, for all three composite variants at temperatures of 23°C, 800°C, 900°C, and 1100°C. It is evident that for $\dot{\varepsilon} \gtrsim 4 \times 10^2$, the strength of 0° and 0/90 material increases very rapidly with $\dot{\varepsilon}$, according to $\sigma_c \propto \dot{\varepsilon}^{\sim 0.77}$. For the 45/45 orientation, on the other hand, $\sigma_c \propto \dot{\varepsilon}^{\sim 0.3}$. For all three configurations, there appears to be a trend for the strength in this $\dot{\varepsilon}$-regime to be slightly lower for $T \gtrsim 800$, but to obey essentially the same $\sigma_c(\dot{\varepsilon})$ function; i.e., n is roughly identical for T = 23°C to 1100°C.

In addition, the threshold strain rate $\dot{\varepsilon}_T$ for the transition to rate-sensitive behavior varies over an order of magnitude, increasing from a minimum of $\dot{\varepsilon}_T \simeq 10^2$ for 45/45 Compglas to $\dot{\varepsilon}_T \simeq 10^3$ for 0° material. The relative ordering of strength for the three variants $(\sigma_c^{0} > \sigma_c^{0/90} > \sigma_c^{45/45})$ at lower strain rates has been reported and discussed elsewhere[1]. In the present context, it is useful to note that even at the lowest strain rate, for which the influence of

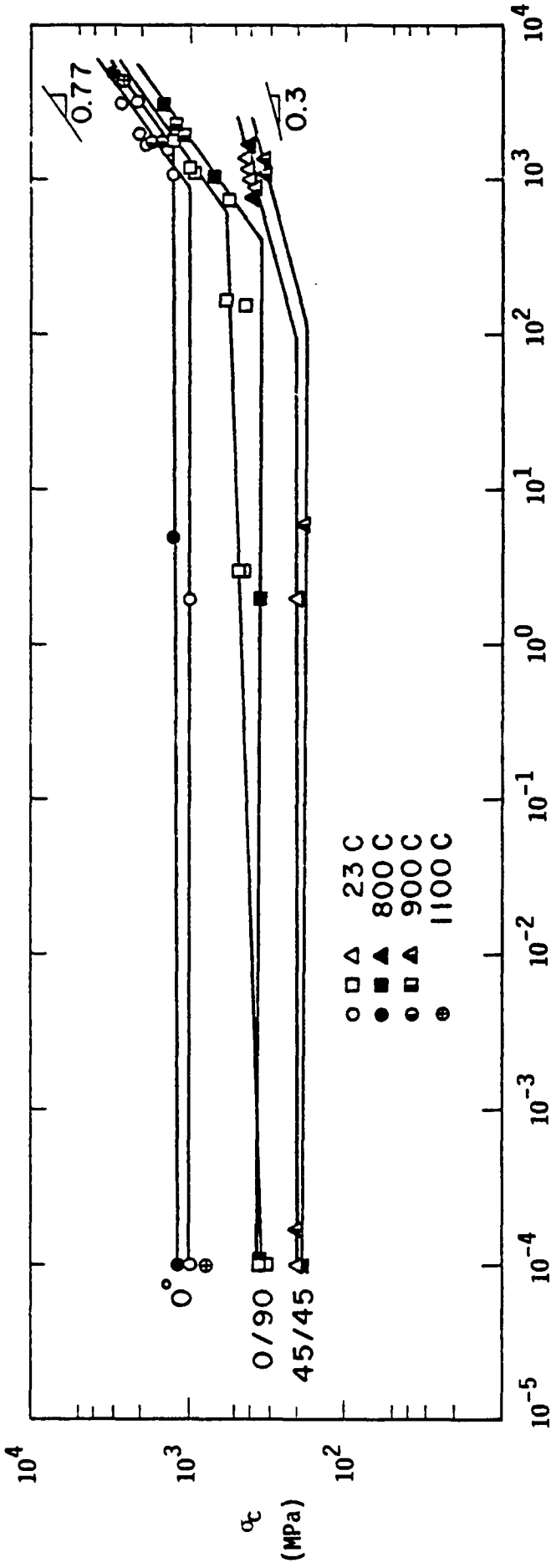

Figure 1(a). Compressive Strength Versus Strain Rate (Compglas)

temperature would be expected to be most pronounced, the strength of 0° material at 1100°C is only slightly lower than that at 23°C. This behavior will be seen to contrast sharply with that of monolithic pyroceram.

It was shown earlier[8] that at low strain rates, Compglas fails in compression by general matrix microfracture, which accommodates general buckling and eventual, localized kinking (failure). It was further observed[1] that at strain rates on the order of 10^3, buckling of damaged but unfailed specimens begins at the surface. Study of specimens used in the present work indicates that at such rapid rates of loading, there is insufficient time for the buckling process to proceed throughout the specimen, and the latter actually fails by forming inhomogeneous kinks, which propagate in narrow, localized shear bands across multiple fiber bundles[9].

The strength-strain rate behavior of pyroceram is shown in Fig. 1b. Over most of the strain rate range ($\dot{\varepsilon} \lesssim 2 \times 10^3\ s^{-1}$), σ_c is essentially constant for temperatures $\gtrsim$ 800°C. However, for T = 1100°C, strength is very strain rate sensitive; at $\dot{\varepsilon} = 10^{-4}\ s^{-1}$, in fact, σ_c is reduced by approximately an order of magnitude compared to that at 23°C, while at $\dot{\varepsilon} = 3 \times 10^3\ s^{-1}$, these strength values are nearly equal. Moreover, room temperature HPB data suggest that during rapid loading, σ_c increases according to $\dot{\varepsilon}^{0.3}$, similar to the results obtained for 45/45 Compglas. It is interesting to note that the average strength of the unreinforced pyroceram is nearly twice that of the strongest (0°) Compglas variant, and that $\dot{\varepsilon}_T$ for the monolithic material is likewise greater than that of any Compglas.

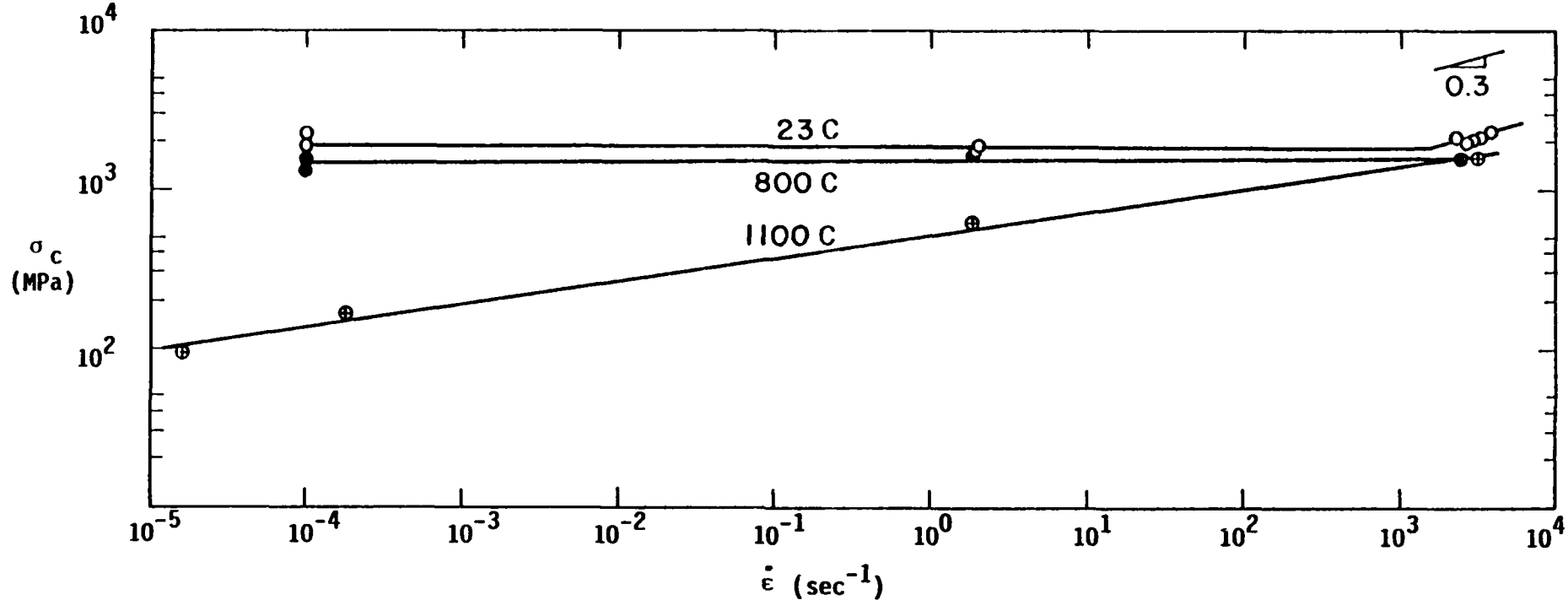

Figure 1(b). Compressive Strength Versus Strain Rate (Pyroceram)

Some understanding of the mechanisms which may be responsible for the foregoing observations can be realized by considering the details of damage development and failure obtainable at low strain rates. Shown in Figure 2 is the stress-strain curve for a pyroceram specimen tested at $\dot{\varepsilon} = 1 \times 10^{-4}\ s^{-1}$ and T = 23°C; also plotted is the cumulative total of acoustic emission events as a function of strain. The loading curve deviates from its initial linear slope at a stress (σ_y), significantly higher than that associated with a major increase in acoustic emission activity above the original background count rate. Subsequent stress-strain is linear, but with a distinctly lower-than-initial slope. Failure is catastrophic; i.e., the specimen is reduced to fine powder.

Such results for a number of specimens tested at $\dot{\varepsilon} = 1 \times 10^{-4}\ s^{-1}$ over a wide range in temperature are summarized in Figures 3 and 4 for pyroceram and 0° Compglas, respectively. As the temperature rises, σ_c for the pyroceram (Figure 3) is constant until T ≃ 600°, at which point the strength experiences a precipitous decline; at 1100°C the strength is more than an order of magnitude lower than at 23°C. This behavior is essentially mirrored by the yield strength and the acoustic emission threshold stress σ_{AE}. At elevated temperature, the σ_y and σ_{AE} curve cross over, and at 1100°C, $\sigma_{AE} = \sigma_c$.

Microscopy reveals that above 800°C, grain boundary sliding is the prevalent mode of deformation. However, the mechanism responsible for the rapid decrease in yield strength between 600°C and 800°C did not manifest itself in terms of surface markings via either optical or scanning electron microscopy.

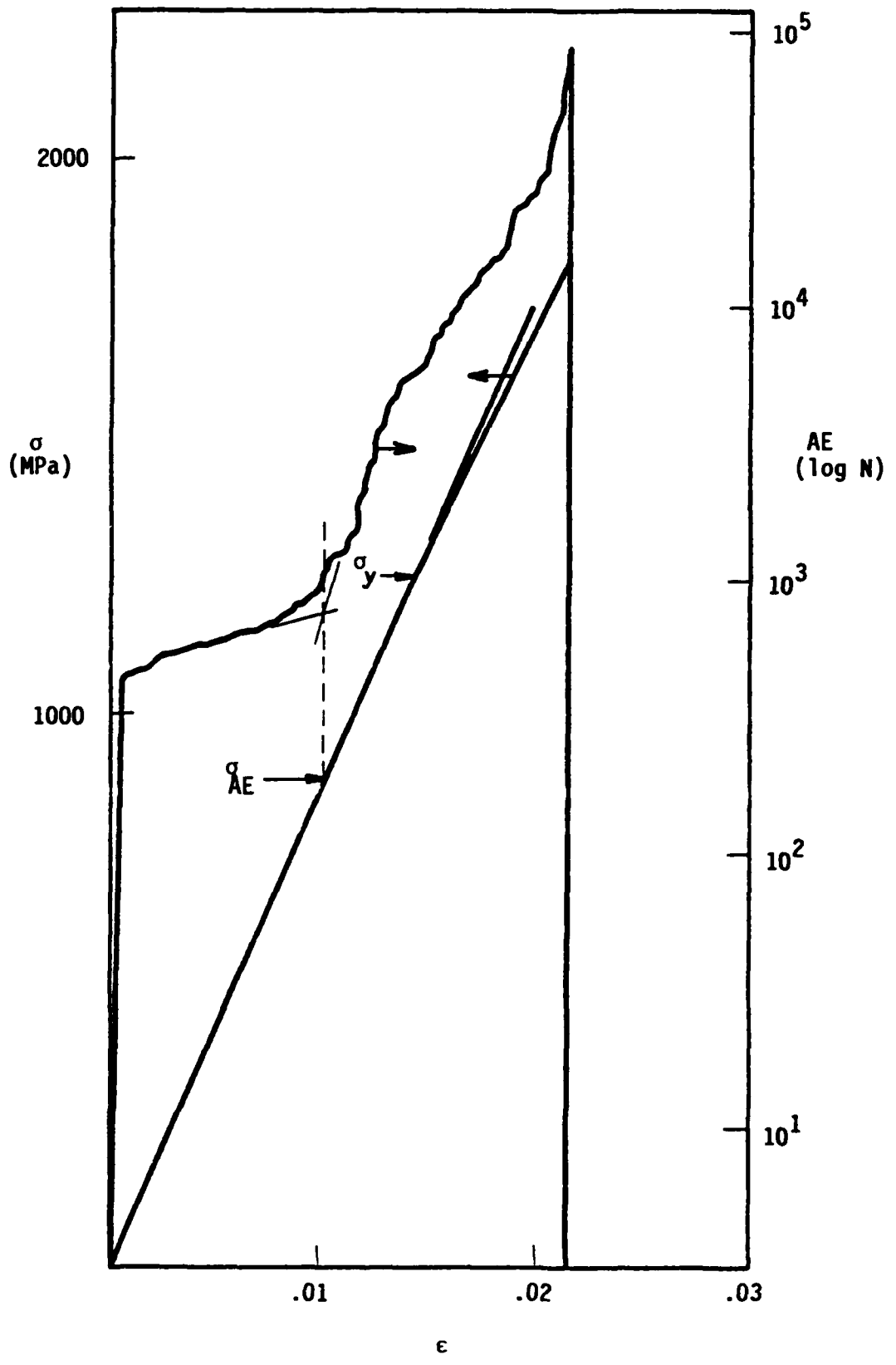

Figure 2. Stress and Acoustic Emission Versus Strain for Pyroceram at $\dot{\varepsilon} = 1 \times 10^{-4} s^{-1}$ and T = 23°C

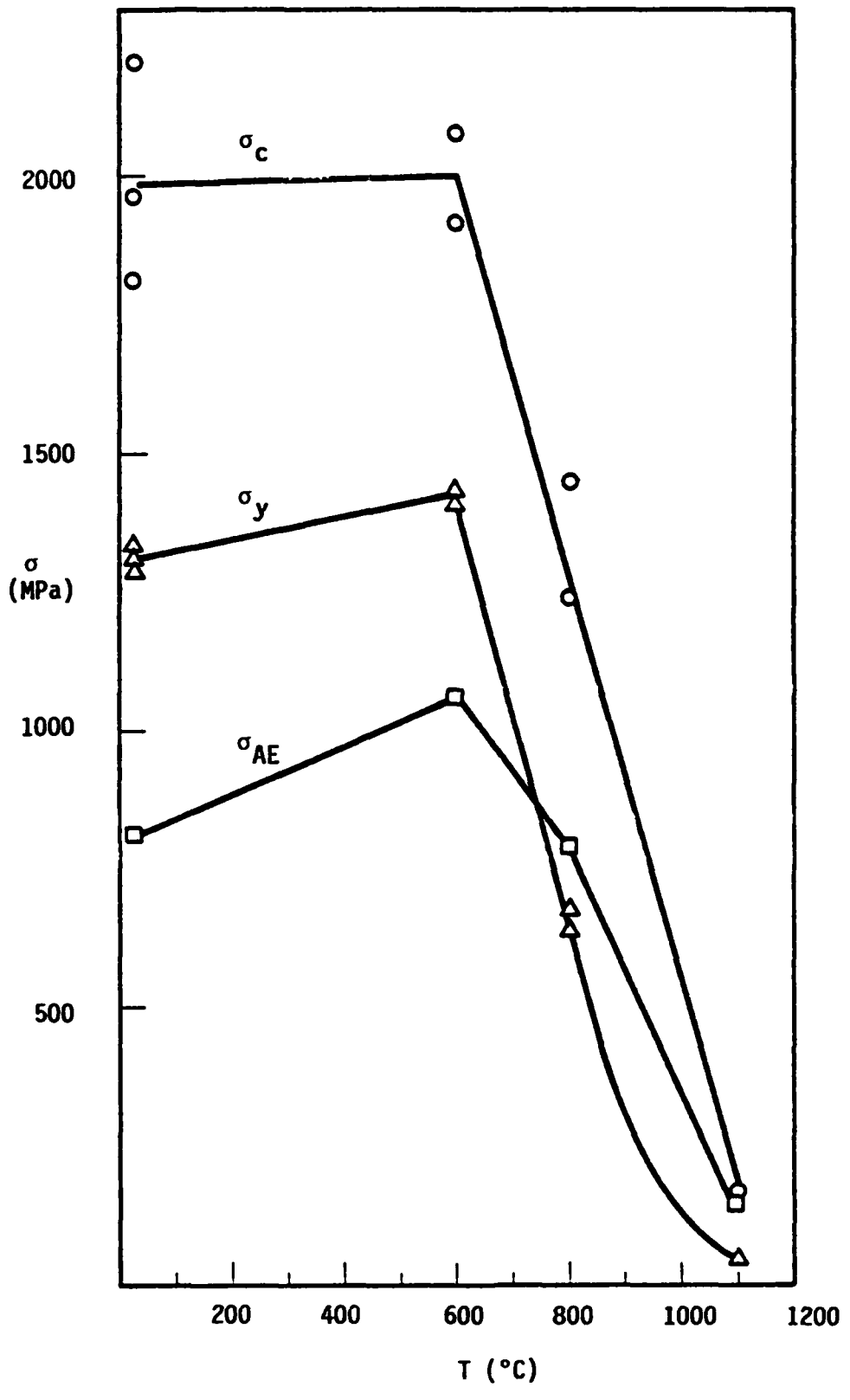

Figure 3. Strength Versus Temperature for Pyroceram

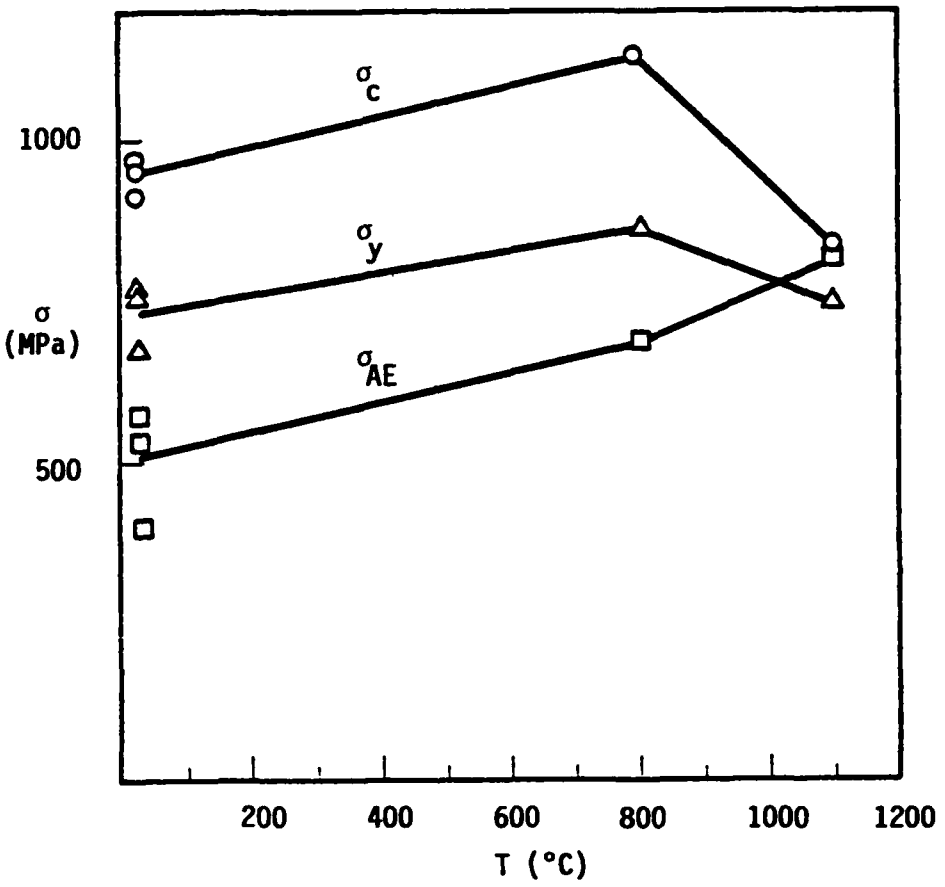

Figure 4. Strength Versus Temperature for 0° Compglas

For purposes of comparison, the behavior of 0° Compglas is shown in Fig. 4. Here it can be seen that all three strength parameters increase proportionately with temperature until $T \approx 800°C$, at which σ_c and σ_y begin to decline. It should be noted that this decline occurs at a higher temperature than was the case for monolithic pyroceram (600°C) and the drop in strength with further increase in temperature is much more gradual.

Finally, Fig. 5 summarizes strength versus temperature for 0° Compglas and pyroceram tested in compression, flexure, and tension (Compglas only); several factors in this representation are noteworthy. It is evident that the compressive and flexural strengths of Compglas are nearly identical, while the compressive strength of pyroceram is much higher, but increases with temperature (for $T \lesssim 600°C$) like that of the former. On the other hand, the tensile strength of Compglas, and the flexural strength of pyroceram are fairly low, and decrease monotonically with increasing temperature. The possible significance of this behavior will be discussed in the following section.

IV. DISCUSSION

The strain rate hardening exponents measured for 0° and 0/90 Compglas at $\dot{\varepsilon} \gtrsim 4 \times 10^2\ s^{-1}$ are, to the knowledge of the author, the highest ($n \approx 0.77$) ever reported. Since the same results are not found for 45/45 Compglas or for pyroceram ($n \approx 0.3$ for both), it would appear that this difference must relate to the fact that the 0° and 0/90 materials offer support in the axial (load) direction by means of their 0° fibers or bundles. Currently, there is no model which is capable of

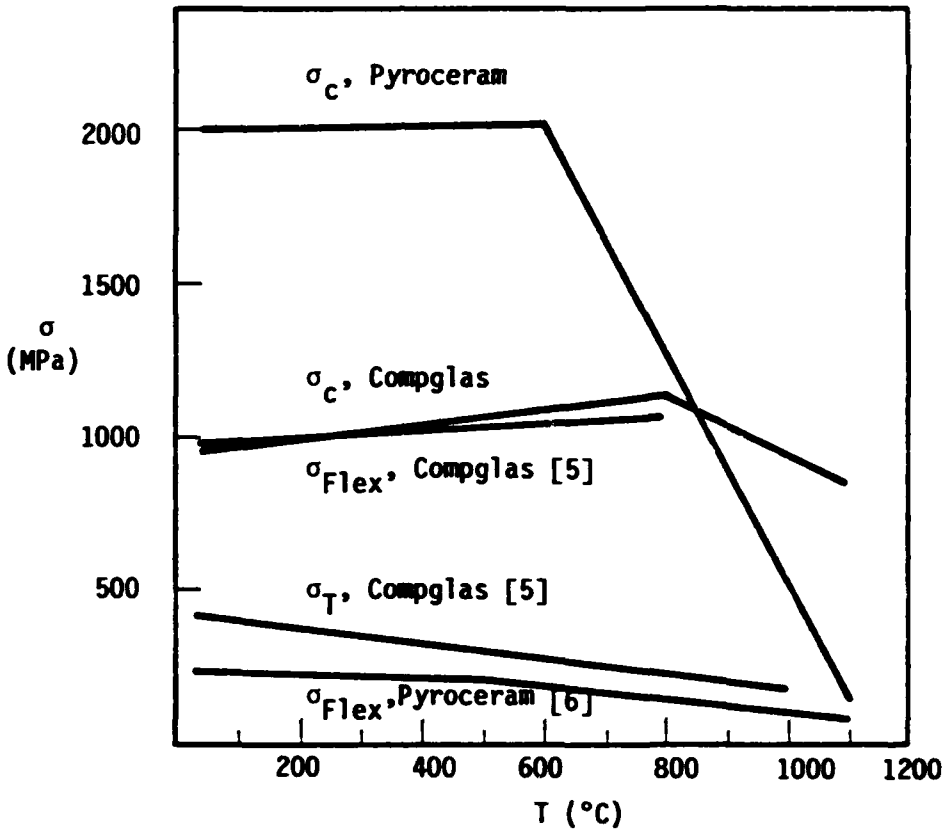

Figure 5. Dependence of Failure Strength Temperature and Loading Made for 0° Compglas and Pyroceram

predicting such high n values, although it is assumed that they derive at least in part from the finite time required for narrow kink bands[9] to propagate across the specimen width. Their significance lies in the fact that they indicate the potential for realizing extremely high damage resistance under shock loading conditions.

It has been observed[1,8] that composite failure under compression requires that the specimen kink and/or buckle, processes which must be accommodated by the matrix. The latter must either flow plastically, or microfracture at the kink/buckle site so that the microfragments can slide and rotate relative to one another. Consequently, matrix yielding or microfracture would appear to be the factor which constrains axial fibers from otherwise kinking or buckling.

From Fig. 1, it is clear that pyroceram tends to soften at elevated temperatures ($T \gtrsim 800°C$), but is strengthened at high loading rates; this helps provide lateral (anti-kink) support to rapidly loaded Compglas. Thus, at high loading rate, n is approximately 0.77 for 0° and 0/90 Compglas at both room and elevated temperature (Fig. 1a).

However, it is interesting to observe that the strength of 0° Compglas at $\dot{\varepsilon} \simeq 1 \times 10^{-4}$ (Fig. 1a) is essentially independent of temperature, despite the fact that the strength of its matrix (Fig. 1b) has dropped from ~ 1500 MPa at T = 800°C, to ~ 150 MPa at 1100°C. Evidently, not much constraint is needed to restrain the kinking process. Since the matrix strength is so temperature sensitive, while that of the composite is not, the strength of 0° and 0/90 Compglas must be controlled primarily by micromechanical factors such as lay-up configuration and the statistics of fiber bending and misalignment. If

so, then matrix yielding/microfracture is not a constraint, but rather simply an accommodation, factor. It follows that high values of n derive principally from difficulty in nucleating and propagating kinks at very high loading rates.

For 45/45 Compglas, the dynamic situation is much closer to that represented by monolithic pyroceram. In both cases, n at high strain rates is on the order of 0.3, which is essentially the value (0.33) predicted by theories based on crack inertia. In the latter, it is assumed that the specimen fails by the nucleation of multiple microcracks, whose subsequent growth and coalescence causes failure. Since the SiC fibers in the Compglas lie at an angle to the applied axial load, they serve as tiny anvils[8] to produce axial microcracks at stresses lower than those required to nucleate similar cracks in the absence of the fibers; i.e., monolithic pyroceram. Hence, the compressive strength of 45/45 Compglas is much less than that of pyroceram at all strain rates (Fig. 1).

Similar arguments can be made for 0/90 Compglas; however, in this case, SiC "anvils" nucleate matrix cracks within roughly half the specimen volume, rather than all of it as for 45/45 Compglas. Therefore $\sigma_c^{0/90} > \sigma_c^{45/45}$. For 0° Compglas, it appears that the critical stress for buckling is less than the stress for homogeneous microfracture in pyroceram, so $\sigma_c^{pyroceram} > \sigma_c^{0^o}$. Current models[10] for fiber kinking/buckling in unidirectionally reinforced brittle matrix composites are incapable of predicting measured 0° Compglas compressive strengths, even at quasi-static rates of loading.

It should be noted that the stress-strain behavior observed for pyroceram (Fig. 2) is extremely unusual for a nominally brittle ceramic. While Compglas also yields, it does so at much lower stress levels, and the process can be related to flexure of the reinforcing fibers, with an attendant reduction in the modulus; in the latter case, "yielding" is really only apparent. Pyroceram, however, appears to exhibit some sort of true yielding, which does not manifest itself in other monolithic technological ceramics, such as SiC, Si_3N_4, and Al_2O_3.[3] Since it is unlikely that the crystalline grains themselves are deforming plastically, it would appear that the most likely mechanism to explain the observed yielding is either viscoelastic flow of glassy material within the grain boundaries, or enhanced compliance due to microcrack opening.

However, it will be recalled that the yield strength for pyroceram exceeds σ_{AE}, the acoustic emission stress level generally associated[1,3] with the threshold for microfracture. Furthermore, even in cases in which microcracking has occurred on a large scale, and in which the average microcracks were quite large relative to the microstructure, no non-linearity was observed in the elastic load line. consequently, it appears that microfracture cannot explain the present results. The most likely candidate, therefore, is intergranular viscoelastic flow.

From the temperature dependence of the strength parameters at low loading rates, it can be inferred that for both the pyroceram (Fig. 3) and Compglas (Fig. 4), σ_y and σ_c are correlated. However, as outlined above, the two materials yield and fail in totally dissimilar fashions. For pyroceram, the precipitous decline in σ_y for $T > 600°C$ has catastrophic consequences for σ_c, since this probably represents the onset of

intergranular flow, as observed[9] microscopically for T = 1100°C. The latter grain boundary sliding produces intergranular cavities, which coalesce to form grain-sized microcracks, which in turn coalesce at failure. Since these processes involve viscous flow, stress wave emission is negligible, so that acoustic emission at elevated temperature is only detected at the failure event; i.e., $\sigma_{AE} = \sigma_c$ at T = 1100°C. At this temperature, σ_c is only a little greater than the flexural strength (Fig. 5), since under both conditions, the specimen fails by multiple microcrack link up. At lower temperatures, $\sigma_c >> \sigma_{Flex}$, since tensile (flexural) failure of monolithic ceramics requires the nucleation of only one dominant (weakest link) microcrack. Compressive failure, however, occurs by the nucleation and coalescence of multiple axial microcracks; the weakest link concept is not relevant, since the first crack to form (when $\sigma = \sigma_{AE}$) is essentially stable even at much higher stress levels.

For Compglas, on the other hand, σ_y represents the stress level for the beginning of fiber flexure, the precursor of fiber/fiber-bundle buckling and kinking. The stress for such flexure is far below that for matrix yielding, so that the latter is not a controlling factor in the flexure process. For this reason, σ_c and σ_y are not greatly affected by temperature, and even at 1100°C, σ_c and σ_y are roughly equal to their respective room temperature values. At the same high temperature, the strength of the pyroceram matrix is lower than that of the Compglas by nearly an order of magnitude.

It is interesting to note that in Fig. 5, the temperature dependence of the tensile strength of Compglas reflects that of σ_{Flex} for pyroceram, suggesting the importance of tensile matrix microfracture in the pure

tensile failure of Compglas[11]. The curve for σ_T of the Compglas can be moved up by increasing the tensile strength of the fibers[5], which bridge tensile matrix microcracks[11] and whose failure ultimately causes failure. And it obviously can be moved down, by removing the fibers, or by decreasing their strength. However, the compressive and flexural strengths of Compglas are almost identical, reflecting the fact that during flexure, the composite fails on its compressive side[5].

V. CONCLUSIONS

SiC fiber-reinforced glass-ceramic composites have the potential for great strength under impulsive loading. This strengthening, which occurs very rapidly with increasing strain rate, has its origin in the rate dependence of kink band initiation and propagation. The effect is basically temperature independent, and the influence of the matrix upon the strain rate hardening exponent is probably secondary to that of the kink process itself. Both the rate of strain rate hardening, and the threshold strain rate for the onset of such hardening, can be controlled by microstructural alteration.

ACKNOWLEDGMENTS

The careful experimental work of A. Nicholls is greatly appreciated, and the support of the Office of Naval Research under Contract N00014-84-C-0213 is gratefully acknowledged.

REFERENCES

1. Lankford, J., "Temperature, Strain Rate, and Fiber Orientation Effects in the Compressive Fracture of SiC Fiber-Reinforced Glass Matrix Composites," Composites, Vol. 18, No. 2 (1987), pp. 145-152.

2. Kipp, M.E., Grady, D.E., and Chen, E.P., "Strain-Rate Dependent Fracture Initiation," International Journal of Fracture, Vol. 16, No. 4 (1980), pp. 471-478.

3. Lankford, J., "The Role of Subcritical Tensile Microfracture Processes in Compression Failure of Ceramics," Fracture Mechanics of Ceramics, Vol. 5, Ed. R.C. Bradt, A.G. Evans, D.P.H. Hasselman, and F.F. Lange, Plenum Press, NY (1983), pp. 625-637.

4. Lankford, J., "Inertia as a Factor in the Dynamic Strength of Brittle Materials," Journal of the American Ceramic Society, Vol. 65, No. 8 (1982), p. C-122.

5. Prewo, K.M.,"Advanced Characterization of SiC Fiber Reinforced Glass-Ceramic Matrix Composites," ONR Technical Report, Contract No. N00014-81-C-0571 (June 1983).

6. Larsen, D.C., "Property Screening and Evaluation of Ceramic Turbine Engine Materials," AFML Technical Report, Contract No. F33615-75-C-5196 (March 1979).

7. Brennan, J.J., "Additional Studies of SiC Fiber Reinforced Glass-Ceramic Matrix Composites," ONR Technical Report, Contract No. N00014-82-C-0096 (April 1984).

8. Lankford, J., "Compressive Strength and Damage Mechanism in a SiC-Fiber Reinforced Glass-Ceramic Matrix Composite," Proceedings of the Fifth International Conference on Composite Materials (ICCMV), eds. W.C. Harrigan, J. Strife, and A.K. Dhingra, TMS-AIME, Warrendale, PA (1985), pp. 587-602.

9. Lankford, J., "Compressive Failure Mechanisms in Ceramic Fiber-Reinforced Ceramic Matrix Composites," Journal of Materials Science (in preparation).

10. Piggott, M.R., "A Theoretical Framework for the Compressive Properties of Aligned Fibre Composites," Journal of Material Science, Vol. 16, No. 10 (1981), pp. 2837-2845.

11. Luh, E.Y., Evans, A.G., "High-Temperature Mechanical Properties of a Ceramic Matrix Composite," Journal of the American Ceramic Society, Vol. 70, No. 7 (1987), pp. 466-69.

Advances in Structural Ceramics (in press)

II.

DEFORMATION OF TRANSFORMATION TOUGHENED ZIRCONIA

JAMES LANKFORD

Southwest Research Institute
San Antonio, TX 78284

Abstract

Recent experimental work on the yield and flow behavior of both single crystal and polycrystalline transformation toughened zirconia is presented. In addition, related work by other researchers is reviewed. The resulting picture is used to assess the relative plastic deformation contributions of phase transformations, dislocation activity, and grain boundary sliding. Particular emphasis is placed on the effects of stabilizer chemistry, grain size, temperature, strain rate, and state of stress. The results are shown to reflect the strong role of shear stresses in selecting, and controlling the operation of, each deformation mode.

I. INTRODUCTION

While the bend strength and fracture toughness of zirconia have received a great deal of attention during the last few years, relatively little effort has been devoted to the study of general deformation in ZrO_2. This is partly due to the fact that aside from experiments performed at elevated temperature, bend testing does not permit a specimen to deform to a significant extent prior to its failing. However, recent studies [1-8] involving compression, in which both deformation and flaw-nucleated non-interacting microcracks are intrinsically stable, has allowed zirconia crystals and polycrystals to attain more-or-less uniform bulk deformation states. Information derived from such experiments can be very useful, since the latter represent what actually obtains in applications (wear, bearings, confined pressure) for which tensile failure is not dominant. Furthermore, the same basic damage mechanisms probably relate to tensile failure as well, but only within the highly localized regions attending crack tips of fracture origins.

The purpose of this paper is to bring together the results of a three-year study of compressive deformation in zirconia at low and intermediate temperatures, parts of which have been recently published [1-4]. This work, combined with the findings of other investigators regarding deformation at high temperature in both tension and compression, provides at least a partial picture of the plastic flow mechanisms, and their influence on strength, for several major types of zirconia alloys. On the other hand, questions persist as to specific slip systems, apparent interaction between competing deformation/transformation modes, and the origins of certain strain rate-temperature effects; these issues will be noted in the discussion.

II. EXPERIMENTAL PROCEDURES

The materials investigated in this study represent several generic zirconia alloy configurations; Table I lists the materials, and some of their relevant properties. These are related to one another as follows.

TABLE 1
MATERIAL PROPERTIES

Material	Grain Size (μm)	Microstructure	Precipitate Vol. %	K_c (MPa$\sqrt{m}$)	Stabilizer
Mg-PSZ[1]	50	C+T	50	9.5	5 MgO
Mg-FSZ[2]	50	C+T (nontransformable)	15	3.7	3.9 MgO
Y-TZP[3]	0.3	T	--	8.5	9 Y_2O_3
Y-FSZ[4]	single crystal	C	--	1.9	20 Y_2O_3
Y-PSZ[4]	single	C+T	50	6.9	5 Y_2O_3

1 Nilsen TS-Grade PSZ; Nilsen Sintered Products, Ltd, Northcote, Victoria, Australia.

2 Supplied by M. V. Swain; CSIRO, Melbourne, Australia.

3 Norton YZ-110 TZP; Norton Co., Northborough, MA, USA.

4 Ceres Corp., Waltham, MA, USA.

The Mg-PSZ material is a classic coarse-grained, cubic (C) matrix, metastable tetragonal (T) precipitate, transformation toughened zirconia. It clearly contrasts with the coarse-grained Mg-FSZ ceramic, whose tetragonal precipitates are too small to transform under stress, and which therefore should primarily reflect its otherwise cubic microstructure (note the relative values of K_c). Similarly, the behavior of the Y-FSZ single crystal material should reflect the intrinsic deformation of the cubic matrix, absent any grain boundary effects (again note the low value of K_c).

The Y-TZP material, like the Mg-PSZ, is capable of transforming under stress, but possesses extremely fine grains. Both of the latter materials compare with the single crystal Y-PSZ, which represents the intrinsic (no grain boundaries) deformation capability of transformable tetragonal phase in a cubic matrix.

The grain boundaries of the Mg-PSZ and Mg-FSZ were relatively clean [9], although they contain some SiO_2 (10). The intergranular phase of the Y-TZP material was quite complex, i.e., a continuous film composed of Y_2O_3, SiO_2, Al_2O_3, and possibly ZrO_2 [11].

Cylindrical compression specimens were fabricated from these materials and tested at various temperatures and loading rates; sample preparation and test techniques are described elsewhere [1-4]. The single crystals of Y-FSZ were cut so that the compressive load axis lay along <123>, while Y-PSZ specimens were oriented along either <123> or <100>. Stress-strain plots are presented in terms of engineering stress (σ) versus engineering strain (ε); c denotes compression, T tension.

Deformation mechanisms were characterized by means of Nomarski interference microscopy, X-ray diffraction, scanning electron microscopy, and transmission (replica and thin foil) electron microscopy. Space does not permit inclusion of the extensive characterization results per se, most of which are being published elsewhere. Therefore, the following section will emphasize deformation and strength, and the plasticity mechanisms responsible will be introduced via reference.

III. EXPERIMENTAL RESULTS

III.1 Stress-Strain

The deformation behavior of single crystal zirconia is shown in Figure 1. At room temperature, the cubic Y-FSZ material fails in a brittle mode, but as the temperature rises, plastic flow is observed. Microscopic study [3] indicates that this flow is related to extensive wavy slip, which propagates down the specimen in a "front" somewhat like a Luders band; in the case of the ceramic, however, the front is more diffuse than it is for metals, and deformation behind the front is inhomogeneous. The (average) trace of the wavy bands corresponds to slip on {111}, within which shear microcracks eventually form; these probably give rise to the σ-ε serrations, and their coalescence causes ultimate failure.

Deformation of Y-PSZ crystals is extremely sensitive to orientation, as shown in Figure 1(b,c). For the <123> samples, transformation plasticity was observed [3] at 23°C; at higher temperatures, phase transformations still contribute to specimen deformation, but the dominant flow mechanism is now dislocation motion. In this case, slip is very planar [3], and occurs on the single most favored {001}. Shear microcrack formation, and failure, eventually occur within the latter planes.

For crystals with the <100> orientation (Figure 1c), deformation proceeds along a markedly different path. At 23°C, a sudden, stress-dependent, incremental plastic strain occurs prior to brittle failure at a higher stress level. As the temperature is increased, the level required for the strain burst, which has a constant magnitude of 0.0049, decreases. Flow subsequent to the second yield point (load drop) follows a monotonic strain hardening path; its stability and extent

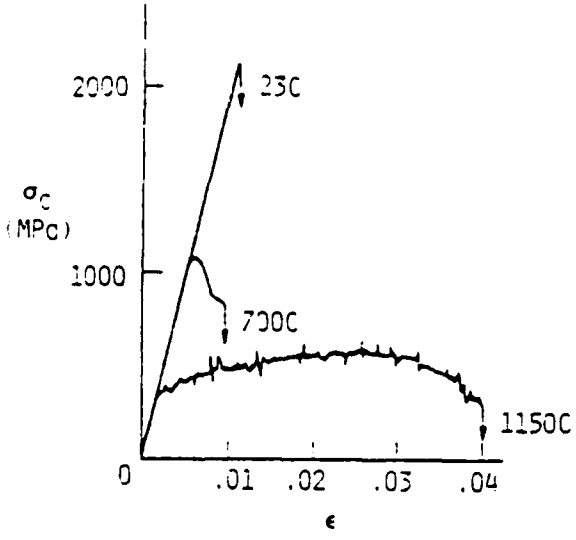

(a) Y-FSZ <123>

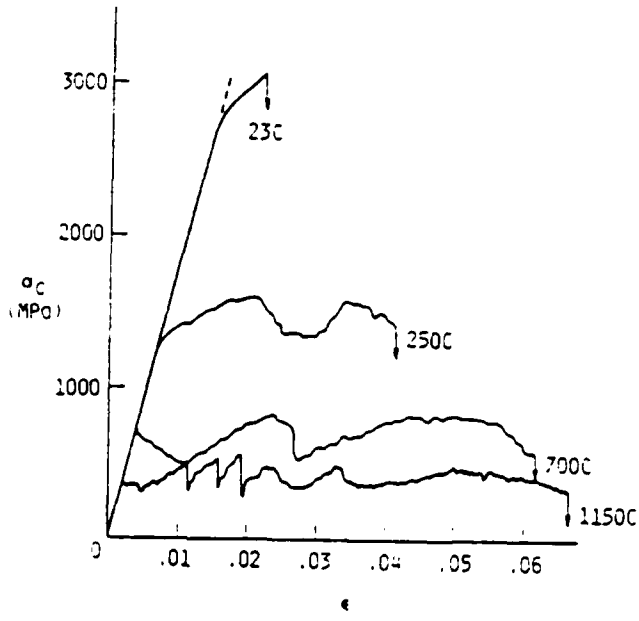

(b) Y-PSZ <123>

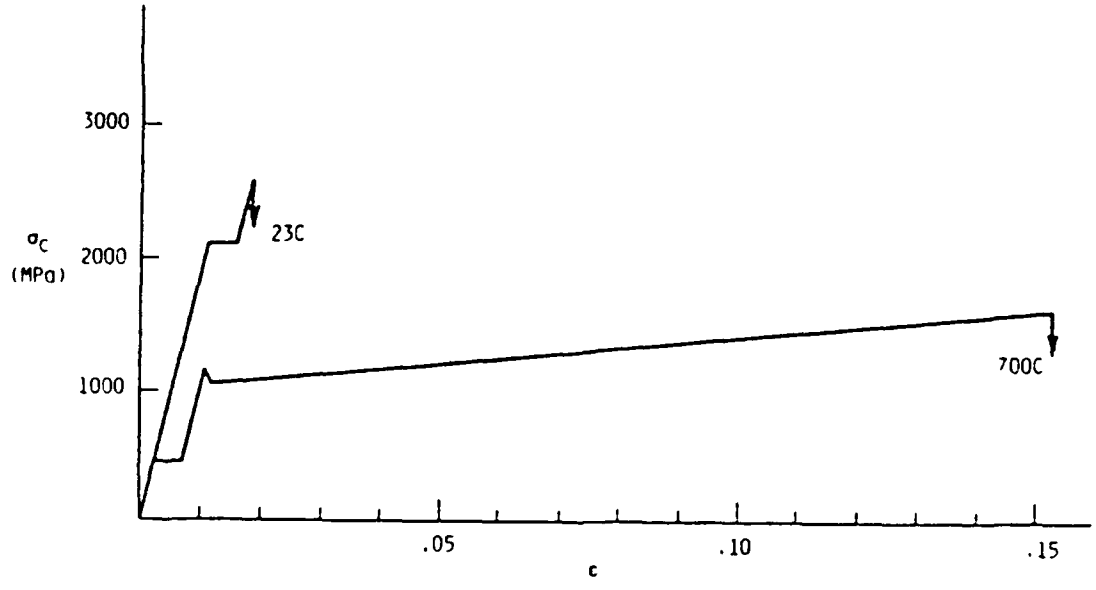

(c) Y-PSZ <100>

Figure 1. Stress-Strain Behavior of Single Crystal Zirconia

(0.15 ultimate strain for T = 700°C) contrast remarkably with the unstable flow, and more limited ultimate strain (0.06) for the <123> orientation at the same temperature.

Based on TEM of surface replicas, it was established [4] that the incremental, pre-macroyield "step" for <100> specimens was caused by the transformation of tetragonal precipitates whose c-axis was parallel to the <100> loading direction. Further, the monotonic hardening, post-yield deformation corresponded to the propagation of a complex Luders front throughout the sample, which failed once the front had encompassed the entire gage section. Thin foil TEM indicated that the deformed region behind the Luders front consisted entirely of two distinct microstructures, i.e., (1) very heavily microtwinned, transformed tetragonal (to monoclinic) precipitates, and (2) a network of highly deformed dislocation cells. The precipitates tended to lie on {110} planes at 45° to the load axis, while the dislocation cell walls appeared to lie in {111} planes. The relative degrees to which these two mechanisms contribute to the hardening is presently unclear.

At still temperatures, the deformation situation becomes simpler, and is fairly well understood [5-7]. Fully stabilized <112> cubic crystals compressed at 1400°C deform via a Luders process (Figure 2a), controlled by solid-solution hardening of the {100}<100> (predominant) and {111}<110> slip systems. Increasing the Y_2O_3 content of the crystals simply enhances the effectiveness of the solution-hardening, and the yield and flow stresses increase accordingly. If the Y_2O_3 content is reduced, the microstructure at 1400°C consists of a cubic matrix with untransformable T-precipitates; the latter lead to precipitation hardening and serrated yielding, which again occurs on {100}<110>. Within this

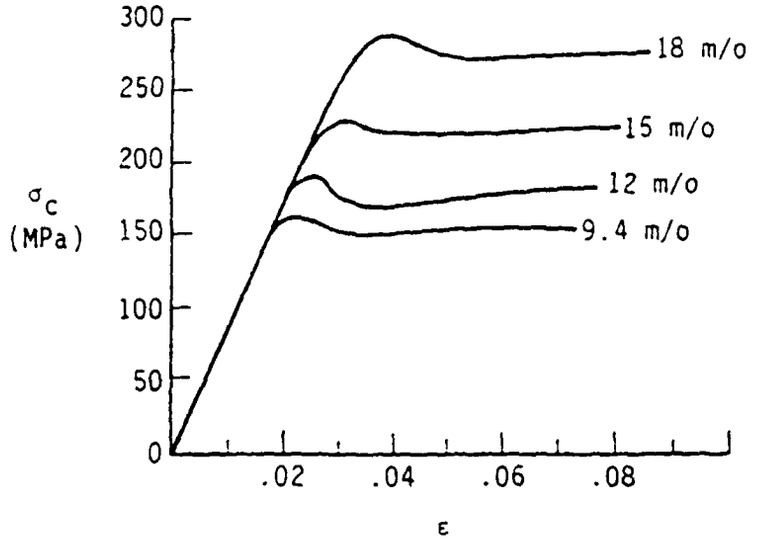

(a) <112> compression axis; T=1400°C; Y_2O_3 content shown for each curve [5].

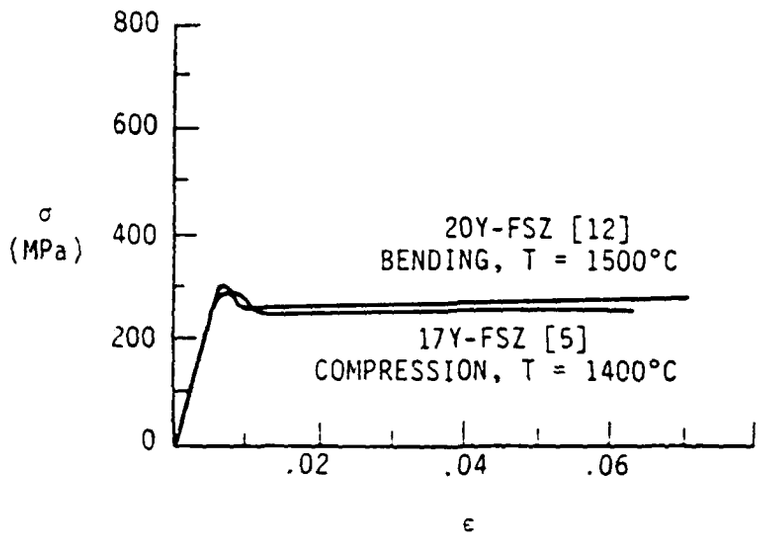

(b) Compression-tension equivalency at elevated temperature.

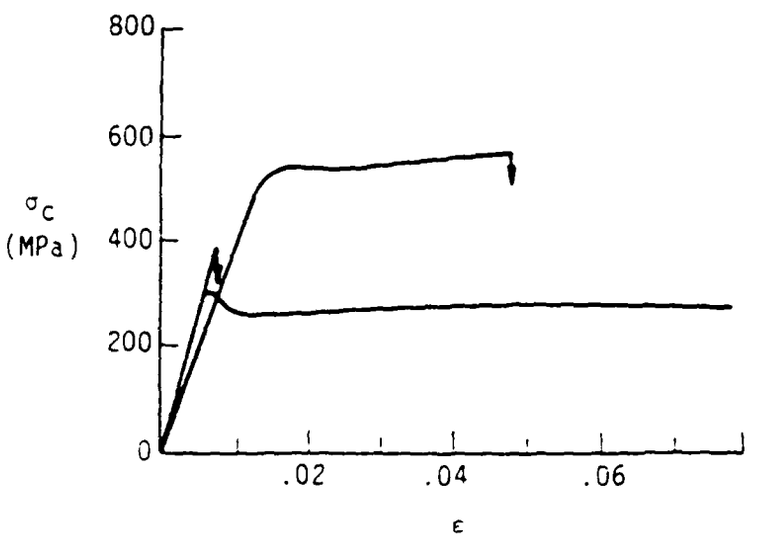

(c) <110> specimen axis; T=1500°C; $\dot{\epsilon} \approx 10^{-4}s^{-1}$ [12]. Strength/ductility differences arise from varying crystallographic orientations relative to bend axis.

Figure 2. Stress-Strain Behavior of Y-FSZ at Elevated Temperature

temperature range, the materials are sufficiently ductile for certain orientations that compression and tension are essentially equivalent, as shown in Figure 2b. However, it is still possible to choose the crystallographic orientation for tension (bending) [12] such that failure is brittle (Figure 2c).

The stress-strain behavior of polycrystalline zirconia both compares and contrasts with that of nominally similar single crystal material, as shown in Figure 3. For example, the essentially cubic (nontransformable) Mg-FSZ material (Figure 3a), is brittle at low temperatures (23°C and 400°C), like the single crystal cubic Y-FSZ. Furthermore, it exhibits a ductility range at 800°C to 1000°C similar to the latter material. However, microscopy shows that the deformation of the polycrystalline zirconia occurs principally via grain boundary sliding and rotation, with concomitant grain boundary cavitation in the glassy grain boundary phase. Grains which cannot slide accommodate the imposed deformation internally by means of wavy slip, presumably on the same slip systems ({111}<110>) [3] involved in the general deformation of the cubic single crystals.

Behavior of the polycrystalline Mg-PSZ (Figure 3b) resembles partially that of the single crystal Y-PSZ, in that it yields and flows at low temperature (23°C) via T → M transformation. However, at 700°C and 1000°C, most of the ductility is accomplished by intergranular creep. Although certain grains do exhibit strain accommodation by transformation plasticity, the strain contribution from this process, as manifested in surface rumpling, clearly declines with increasing temperature. No evidence of dislocation activity could be found either in thin foils or by surface replication.

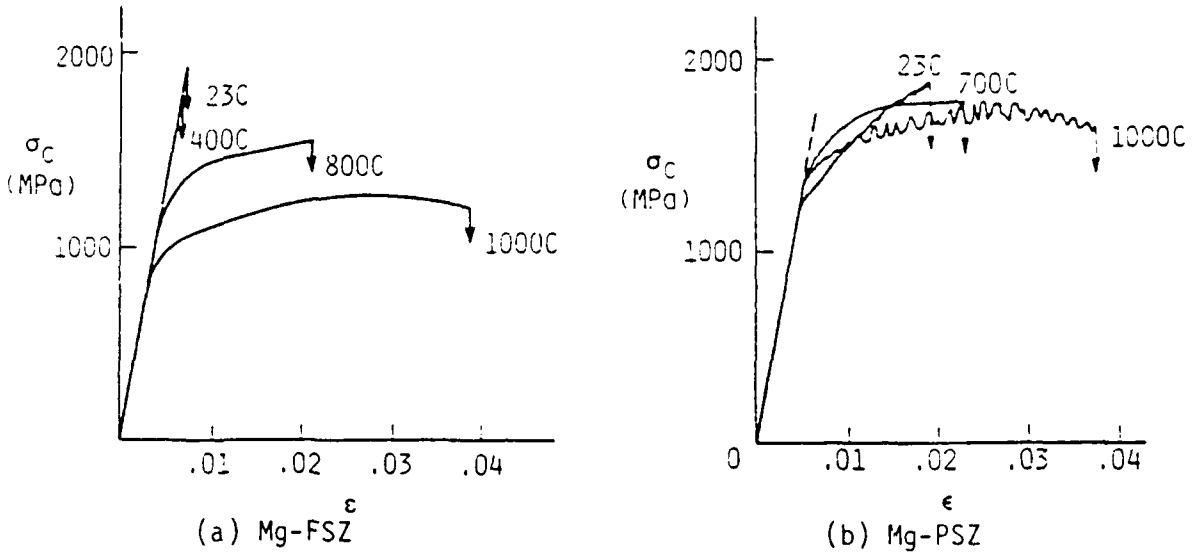

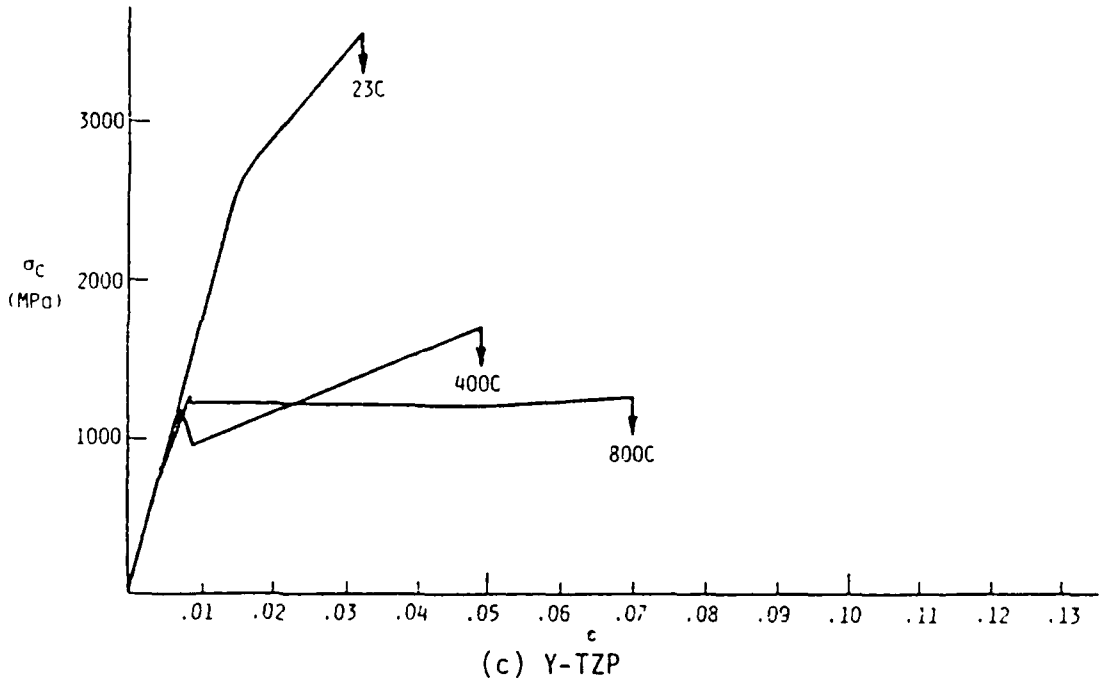

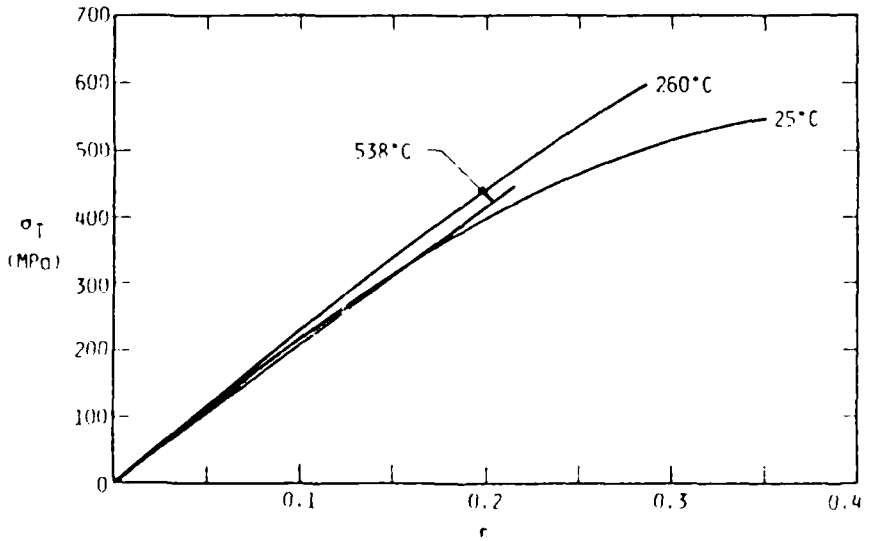

(d) Tensile stress versus flexural strain for Mg-PSZ [13].

Figure 3. Stress-Strain Behavior of Polycrystalline Zirconia

The declination in transformation strain with increasing temperature is underscored by results obtained in bending [13]. Here (Figure 3d) it can be seen that yielding and flow (limited by failure of the specimen) occurs at 25°C, while at 260°C and 538°C the stress-strain curve is perfectly linear to the point of brittle failure. At 25°C the surface of the sample rumples, indicates of transformation plasticity; not so at the higher temperatures.

The Y-TZP material (Figure 3c), like the Mg-PSZ, yielded and deformed at 23°C solely by means of transformation plasticity. At 400°C and 800°C, however, apparent plasticity is caused principally by intergranular flow, i.e., grain boundary sliding. This sliding is a consequence of the intergranular viscous film; it is interesting to note that the properties of the film are such that grain boundary cavities are observed (via TEM replicas) to form at strain rates on the order of $10^{-4}s^{-1}$ [4]. This means that they formed and coalesced within less than about one minute. At both temperatures, net section deformation appears to take place in shear bands, which at 800°C are virtually superplastic (surrounded by elastic enclaves), and at both temperatures, propagate through the specimen as a "Luders" front. At 400°C, the distribution of cavitated and sliding grain boundaries is quite homogeneous, although incipient shear band formation can be imaged by Nomarski contrast.

Not surprisingly, it is possible to achieve true (bulk) superplasticity by deforming samples at still higher temperatures, as found recently by Wakai, et al [8,14]. Figure 4, for example, shows the dependence of creep strain upon time and temperature at a low static stress for an Y-TZP [14] very similar to the one used in the present study. It should be noted that strains on the order of unity can be obtained under such conditions.

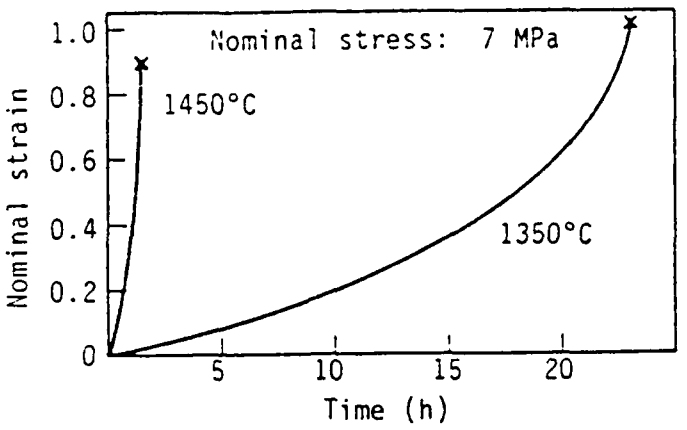

Figure 4. Creep Strain Versus Times at Constant Load for Very Fine-Grained Y-TZP [4]

If the stress-strain results for the Y-TZP are considered in terms of the effect of strain rate at constant temperature, a curious trend emerges. As shown in Figure 5a, specimens tested at 23°C all yield and fail at roughly the same stress level, but the ductility at $\dot{\varepsilon} = 10^{-5}s^{-1}$, for both T = 400°C and T = 800°C, is caused by homogeneous and inhomogeneous grain boundary sliding, respectively.

This behavior contrasts remarkably with that of similar single crystal material. As shown in Figure 5d, Y-PSZ <100> specimens tested at 700°C deform with increasing difficulty as $\dot{\varepsilon}$ increases; the pre-macroyield stress level increases, as does the stress required for bulk flow, and ductility decreases dramatically (it is nil for $\dot{\varepsilon} = 10^{3}s^{-1}$). This represents the inverse strain-rate behavior characteristic of most thermally activated processes, in marked contrast to equivalent results obtained for Y-TZP polycrystals (Figure 5c).

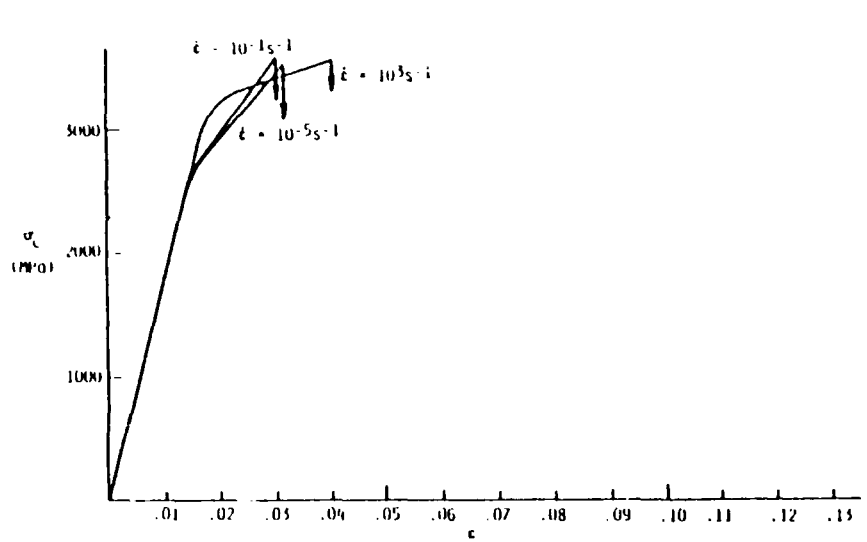

(a) Y-TZP, T=23°C

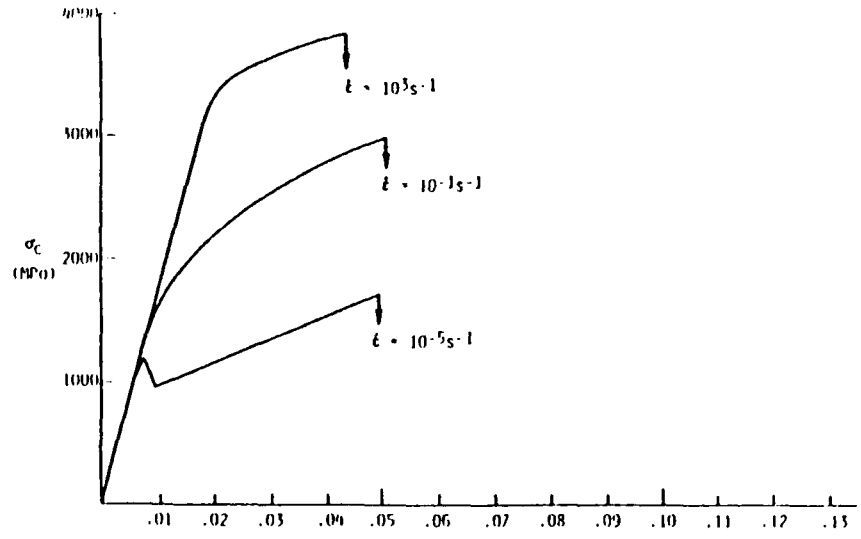

(b) Y-TZP, T=400°C

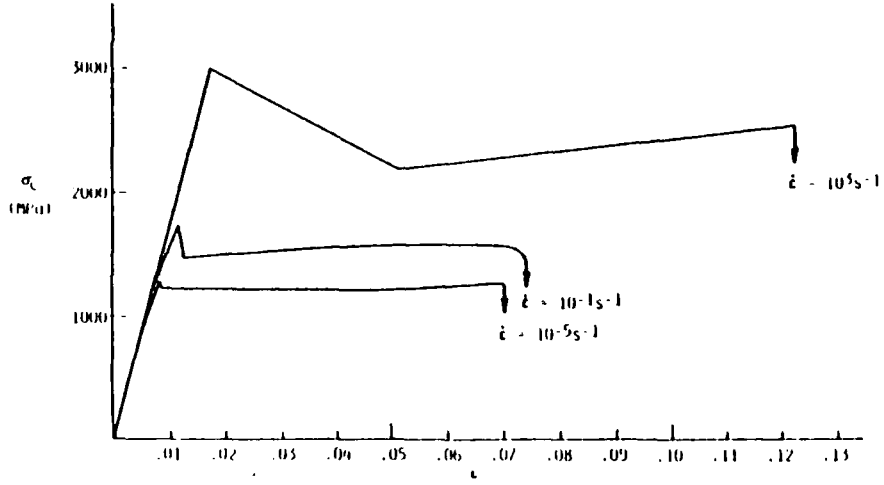

(c) Y-TZP, T=800°C

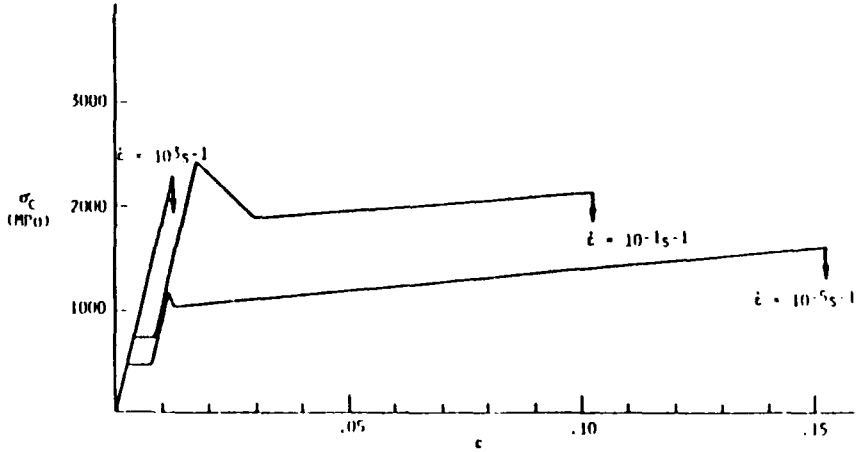

(d) Y-PSZ <100>, T=700°C

Figure 5. Temperature-Strain Dependence of Compressive Yield and Flow in Polycrystalline Y-TZP and Y-PSZ Single Crystals

III.2 Strength-Strain Rate

The strength of most monolithic ceramics has been observed to depend upon strain rate as shown for Si_3N_4 in Figure 6. Below $\dot{\varepsilon} = 5x10^3 s^{-1}$, σ_c increases slowly with $\dot{\varepsilon}$ at a rate which correlates with the thermal activation of small tensile (even for nominally compressive loading) microcracks. Above this loading rate, the strength undergoes a transition to a regime in which the strength increases very rapidly with $\dot{\varepsilon}$, at a rate essentially independent of temperature [15].

This is not what happens in the case of zirconia single crystals. As shown in Figure 7(a-c), σ_c decreases with $\dot{\varepsilon}$ for T = 23°C, while increasing with strain rate, as expected, at 700°C. The existence of the inverse relationship between σ_c and $\dot{\varepsilon}$ at 23°C is apparently independent of the relative degree of stabilization (Figure 7a,b), as well as orientation (Figure 7b,c).

On the other hand, polycrystalline variants behave in a more conventional fashion (Figure 7(d-f)), aside from the fact that the transition to the inertial regime is not clearly observed at high loading rates. Implications of the foregoing results will be explored in the following section.

IV. DISCUSSION

It is evident that both single crystal and polycrystalline zirconia exhibit plastic deformation at remarkably low homologous temperatures, provided the state of stress is such (in the present case, compressive) that samples do not fail prematurely via flaw-nucleated tensile fracture. This has been noted previously by Swain [16] and by Chen and Reyes Morel [17], who considered only the inelastic deformation inherent

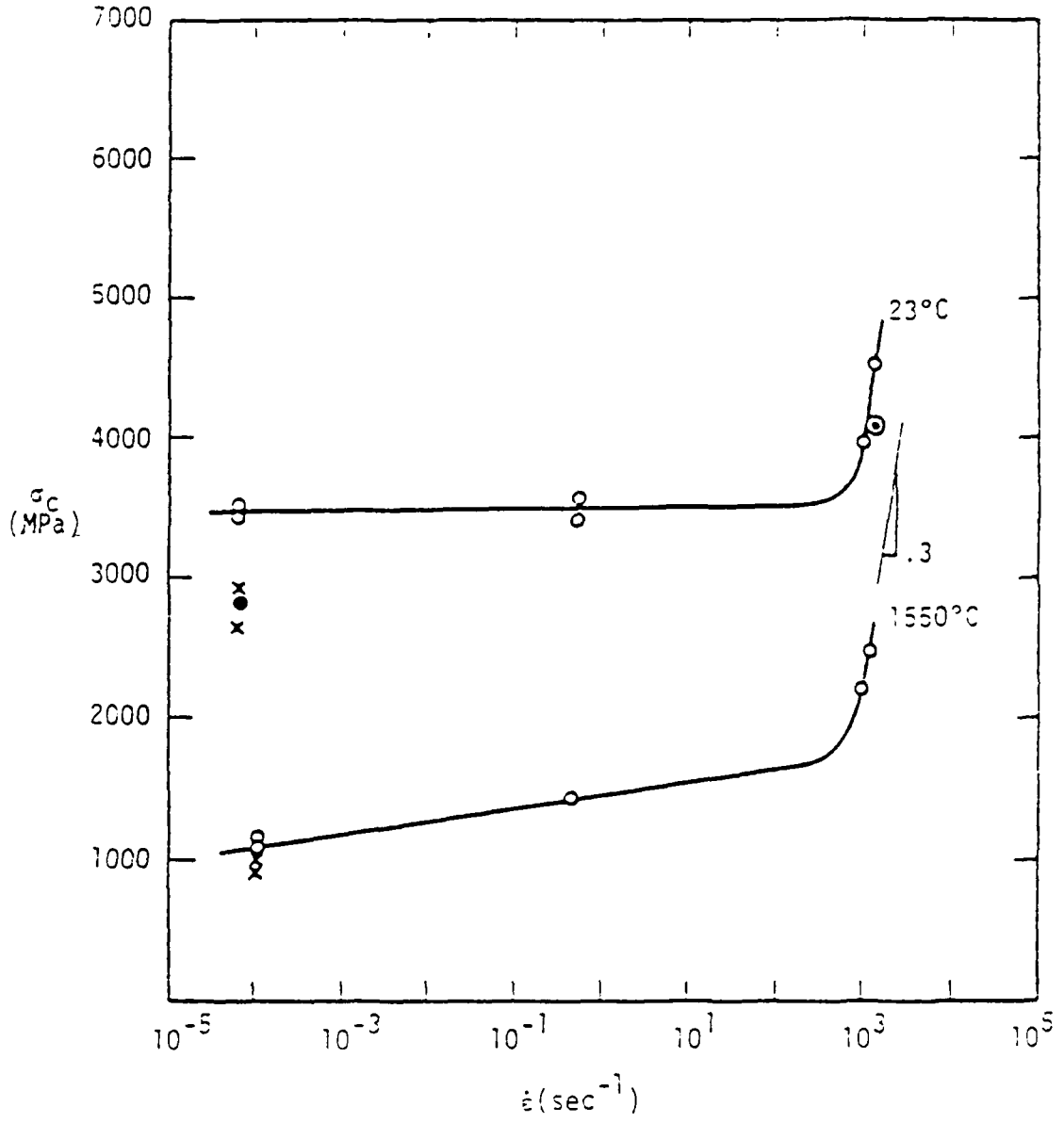

Figure 6. Compressive Strength Versus Strain Rate for Hot-Pressed Si_3N_4

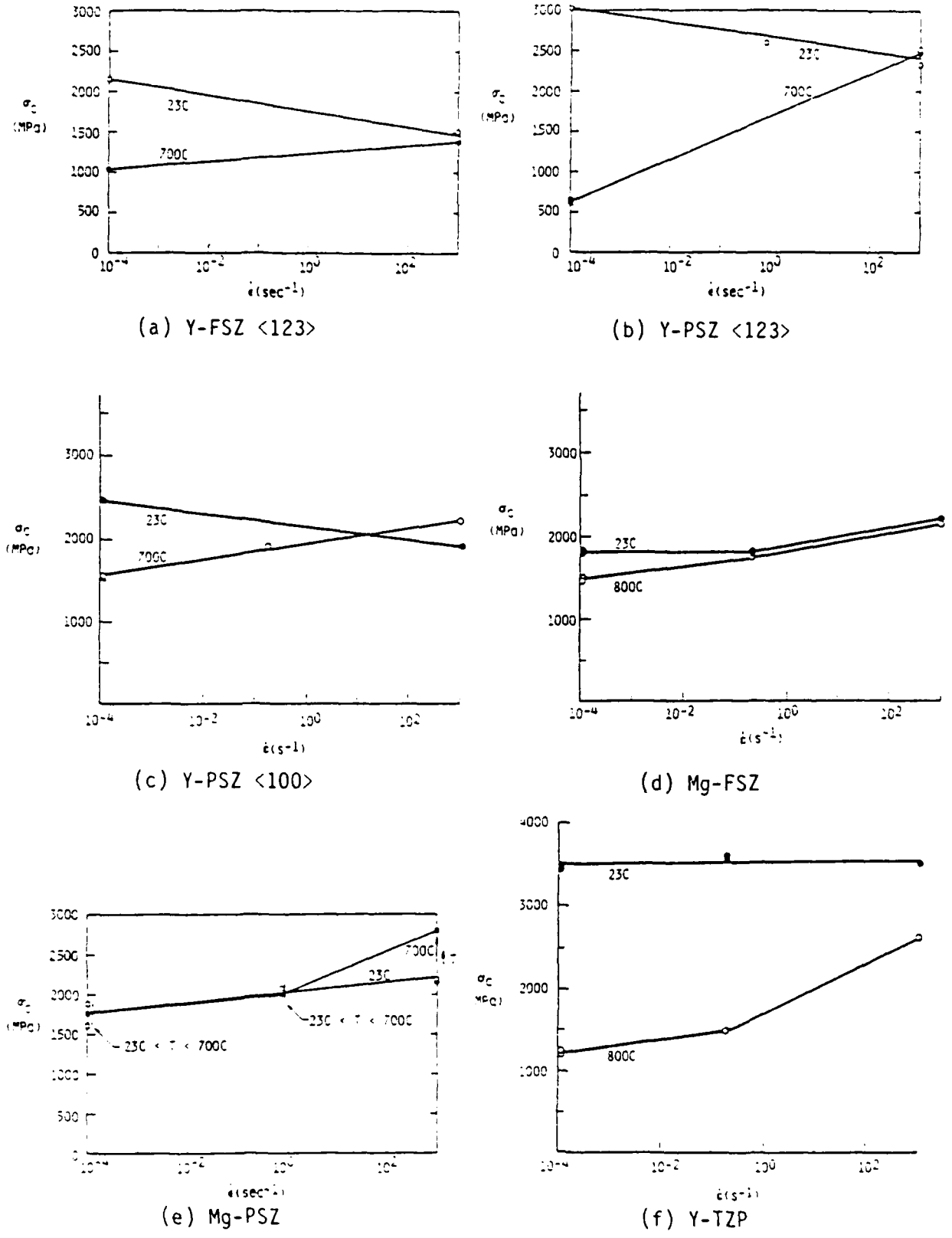

Figure 7. Compressive Strength Versus Strain Rate for Single Crystal and Polycrystalline Zirconia

in transformation plasticity. The present work extends this concept to dislocation slip and grain boundary sliding deformation mechanisms as well. All of these processes are dominated by shear, and their development in zirconia usually represents the onset of micromechanical instability, as manifested in low hardening rates and multiple load drops. Almost every deformation mechanism discussed in this paper (slip and transformation Luders bands in single crystals; autocatalytic transformation bands in polycrystal grains; superplastic shear bands) initiated from local instabilities. Major questions concern how to model the factors which trigger these several deformation instabilities.

For both single crystals and polycrystals, any strain which occurs at room temperature appears to be generated by phase transformations; essentially no dislocation activity is observed. However, dislocations begin to account for most of the observed single crystal strain at temperatures as low as 250°C (Y-PSZ <123>, Figure 1b), while grain boundary sliding is the principal deformation mechanism in polycrystals at temperatures $\geq$ 400°C. As noted earlier, transformation strains in Mg-PSZ are negligible at temperatures no higher than 260°C (Figure 3d [13]). While slip and transformations do occur at these temperatures (250-800°C), they seem to serve principally to accommodate the predominant grain boundary (GB) sliding. Slip observed in polycrystals appears to be qualitatively similar to that characteristic of similar single crystals.

Failure of all of the ZrO_2 polycrystalline variants was caused by the coalescence into cracks of cavities nucleated at multiple sites within viscous films on GB facets. The cavitation is a direct consequence of the sliding of grain boundaries lying at near 45° angles to the applied stress axis. This is reflected in the macroscopic shear bands observed for Y-PZP

at 400°C and 800°C [4]. At 400°C, the GB phase is still sufficiently viscous that only certain boundaries are able to slide at a given stress level; at higher stresses, slightly less favorable boundaries, usually not physically associated with the first to move, are activated. This accounts for the observed hardening and stability of the flow stress curve (Figure 3c). However, at 800°C, many contiguous boundaries can slide at roughly the same flow stress. This produces a low rate of hardening, as "superplastic" bands nucleate and move through the specimen by autocatalysis. It is clear that if the superplastic bands could be prevented, and the GB shear displacements distributed more uniformly, the result would be bulk superplasticity, which has already been achieved at much higher temperatures (1350°C [14]). It is possible that the remarkable increase in both strength and ductility for Y-TZP tested at $\dot{\varepsilon} = 10^3 s^{-1}$ and 800°C (Figure 5c) represents the suppression of instability by the rapid applied loading. This would promote the sliding of many less favorably oriented grain boundaries and inhibit strain localization.

Most of the shear bands which have been observed lie at about 45° to the stress axis. Dalgleish and Evans [16] have attempted to analyze this kind of deformation, and were able to show that to the extent that the macroscopic orientation of the shear bands deviates from 45° relative to the stress axis, the ratio of the GB dilatational strain to the shear strain increases. In the present case, shear bands caused by GB sliding/cavitation invariably lay near 45°, implying that dilatation contributed comparatively little to the macroscopic strain, most of which arose from microscopic GB sliding within the overall plane of the bands.

From Figures 1c and 5d, it is evident that the transformation responsible for the pre-macroyield strain "step" in Y-PSZ <100> crystals is thermally activated. That is, the stress required to initiate the transformation increases with strain rate, and decreases with temperature. It is well known that the transformation supposed to be responsible for inelasticity in these materials is the martensite T → M. The martensite nucleation mechanism responsible for the observed (extreme) temperature-strain rate sensitivity is not known, and merits further study.

It was observed (Figure 7) that at elevated temperatures, the strength of single crystal and polycrystal ZrO_2 increased monotonically. In the case of the former, the increase is due to suppression of thermally activated slip. Similarly, for the large grained polycrystals, the strength was enhanced at higher loading rates by the suppression of viscous GB sliding processes. However, the strength of the fine-grained Y-TZP increased with $\dot{\varepsilon}$ principally because of suppression of instability (shear band) formation.

The basis for the inverse strength-strain rate effect observed for all single crystal variants at 23°C is not yet known. It seems clear, however, that it has nothing to do with transformations, since the effect was present in fully stabilized material (Figure 7a). Since the cracks which cause failure of single crystals have a tendency to lie on certain inclined shear planes, it may be that the sudden imposition of a compressive stress component across the crack face incudes such a large friction stress that the cracks cannot shear, and are forced to propagate in a more axial direction. This change in mode might then cause failure at a lower stress level because of easier crack linking (coalescence).

ACKNOWLEDGMENT

The support of the Office of Naval Research under Contract Number N00014-84-C-0123 is gratefully acknowledged.

REFERENCES

1. J. Lankford, **J. Am. Ceram. Soc.** 66, C212 (1983).

2. J. Lankford, **J. Mat. Sci.** (20), 53 (1985).

3. J. Lankford, **J. Mat. Sci.** 21, 1981 (1986).

4. J. Lankford, L. Rabanberg, R. A. Page, **J. Am. Ceram. Soc.** (submitted).

5. A. Dominguez-Rodriguez, K. P. D. Lagerlof, A. H. Heuer, **J. Am. Ceram. Soc.** 69 281 (1986).

6. A. Dominguez-Rodriguez, V. Lanteri, A. H. Heuer, **J. Am. Ceram. Soc.** 69, 285 (1986).

7. M. L. McCartney, W. T. Donlon, A. H. Heuer, **J. Mat. Sci. Lttrs.** 15, 1063 (1980).

8. F. Wakai, S. Sakaguchi, K. Kanayama, H. Kato, H. Onishi, presented at the Second International Symposium on Ceramic Materials and Components for Engines, Lubeck-Travemunde, Federal Republic of Germany,, 1986 (unpublished).

9. M. V. Swain, **J. Mat. Sci. Lttrs.** 4, 848 (1985).

10. J. Drennan and R. H. J. Hannink, **J. Am. Ceram. Soc.** 69, 541 (1986).

11. M. Ruhle, N. Claussen, A. H. Heuer, in **Science and Technology of Zirconia II**, edited by N. Claussen and A. H. Heuer (The American Ceramic Society, Columbus, OH, 1984), p. 352.

12. R. P. Ingel, D. Lewis, B. A. Bender, R. W. Rice, Com. Am. Ceram. Soc. 65, C150 (1982).

13. D. C. Larsen and J. W. Adams, AFWAL Report No. 10, Contract F33615-79-C-5100, April, 1981.

14. F. Wakai, S. Sakaguchi, Y. Matsuno, Adv. Ceram. Mat. 1, 259 (1986).

15. J. Lankford, Com. Am. Ceram. Soc. 65, C122 (1982).

16. B. J. Dalgleish and A. G. Evans, **J. Am. Ceram. Soc.** 68, 44 (1985).

END

12-87

DTIC